Statistical field theory for nonlinear elasticity of polymer networks with excluded volume interactions

Pratik Khandagale [1,*] Timothy Breitzman,[2] Carmel Majidi [1,3,4] and Kaushik Dayal [1,3,5,6]

[1]*Department of Mechanical Engineering, Carnegie Mellon University, Pittsburgh, Pennsylvania 15213, USA*

[2]*Air Force Research Laboratory, Wright-Patterson Air Force Base, Ohio 45433, USA*

[3]*Department of Civil and Environmental Engineering, Carnegie Mellon University, Pittsburgh, Pennsylvania 15213, USA*

[4]*Department of Materials Science and Engineering, Carnegie Mellon University, Pittsburgh, Pennsylvania 15213, USA*

[5]*Center for Nonlinear Analysis, Department of Mathematical Sciences, Carnegie Mellon University, Pittsburgh, Pennsylvania 15213, USA*

[6]*Pittsburgh Quantum Institute, University of Pittsburgh, Pittsburgh, Pennsylvania 15260, USA*

(Received 20 July 2022; revised 5 April 2023; accepted 17 April 2023; published 2 June 2023)

Polymer networks formed by cross linking flexible polymer chains are ubiquitous in many natural and synthetic soft-matter systems. Current micromechanics models generally do not account for excluded volume interactions except, for instance, through imposing a phenomenological incompressibility constraint at the continuum scale. This work aims to examine the role of excluded volume interactions on the mechanical response. The approach is based on the framework of the self-consistent statistical field theory of polymers, which provides an efficient mesoscale approach that enables the accounting of excluded volume effects without the expense of large-scale molecular modeling. A mesoscale representative volume element is populated with multiple interacting chains, and the macroscale nonlinear elastic deformation is imposed by mapping the end-to-end vectors of the chains by this deformation. In the absence of excluded volume interactions, it recovers the closed-form results of the classical theory of rubber elasticity. With excluded volume interactions, the model is solved numerically in three dimensions using a finite element method to obtain the energy, stresses, and linearized moduli under imposed macroscale deformation. Highlights of the numerical study include: (i) the linearized Poisson's ratio is very close to the incompressible limit without a phenomenological imposition of incompressibility; (ii) despite the harmonic Gaussian chain as a starting point, there is an emergent strain-softening and strain-stiffening response that is characteristic of real polymer networks, driven by the interplay between the entropy and the excluded volume interactions; and (iii) the emergence of a deformation-sensitive localization instability at large excluded volumes.

DOI: 10.1103/PhysRevE.107.064501

I. INTRODUCTION

A wide variety of soft-matter-based systems are emerging as important for engineering and scientific applications, and have been the focus of research using both modeling and experiments, e.g., Refs. [1–32]. Polymer-network-based materials such as elastomers and hydrogels are often at the heart of these soft-matter systems.

An important question for both fundamental understanding and application is how to predict the nonlinear elastic properties of polymer networks starting from a micromechanical model of individual chains. The physics of polymer network elasticity is governed by the conformational entropy of polymer chains and the intersegment excluded volume interactions. These contributions can be roughly thought of as short-range and nonlocal interactions, respectively. The short-range interactions are associated with Gaussian polymer chain response and depend on the relative configurations of adjacent segments in a chain. In contrast, the nonlocal interactions are due to the interaction between polymer segments that are nearby in space but nonlocal topologically [i.e., in terms of their position along the chain (Fig. 1)].

While there are several useful phenomenological nonlinear elastic frame-indifferent models, e.g., Mooney-Rivlin [33], Ogden [34], and Gent [35], they lack a clear connection to the molecular structure of polymer network. An important class of physics-based approaches to study the elasticity of polymer networks are based on considering multiple Gaussian chains and then averaging over the chains in different ways. These include the three-chain model by James and Guth [36], the four-chain model by Flory and Rehner [37] and Treloar [38], the affine full-network model by Treloar [39], the eight-chain model by Arruda and Boyce [40], the nonhomogeneous deformation-based model by Wu and van Der Giessen [41], and the nonaffine microsphere model by Miehe [42]; the recent work by Grasinger [43] provides a new perspective in which these myriad models are shown to be special cases of a general approach. While these models have provided important insights and prediction, they do not account for the nonlocal excluded volume effects. Consequently, incompressibility of the polymer network must be added as a phenomenological continuum-scale approximation of the missing mesoscale physics. Another class of physics-based

*pratik.khandagale701@gmail.com

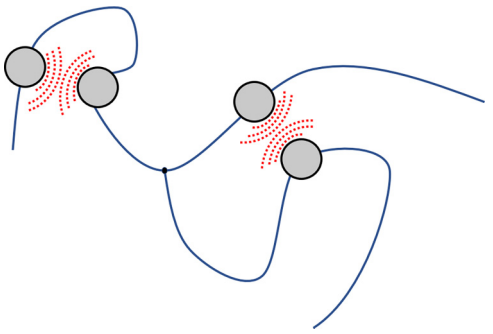

FIG. 1. Excluded volume interactions are nonlocal in terms of the segment coordinates.

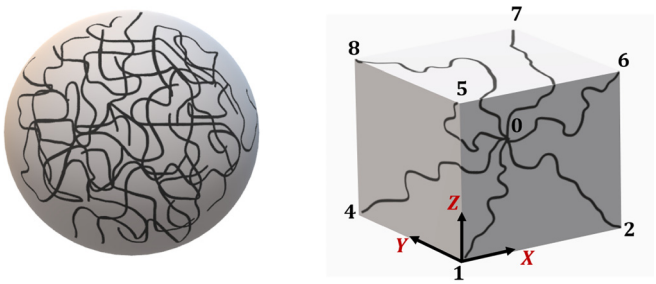

(a) Schematic of a polymer network (b) The 8-chain approximation

FIG. 2. The eight-chain approximation is obtained by averaging over a volume element that aligns the polymer chains along the principal directions of the deformation.

molecular-statistical approaches are the constrained junction and constrained segment theories, that aim to account for constraints arising due to chain entanglements. Constrained junction theories, e.g., Refs. [44–48], apply topological constraints on the fluctuations of chain cross-link junctions. Constrained segment theories, e.g., Refs. [49–53], which are consistent with the tube model of rubber elasticity, incorporate constraints on the polymer segments along the chain contour. However, it is not easy to incorporate the nonlocal excluded volume interactions in these approaches.

A. Proposed approach

Our approach is composed of two key elements: first, the statistical field theory of polymers, which provides an established and efficient approach to account for the physics of polymer chain elasticity as well as excluded volume interactions [54–70]; and, second, the use of the eight-chain network averaging model that provides a nonlinearly elastic frame-indifferent approach to coarse grain to the continuum scale [40]. An important work in this direction is Ref. [71], wherein a network with a simplified square lattice topology was studied using the field theory approach to understand copolymers.

We begin by considering a representative volume element (RVE) of the polymer network. A typical mesoscale RVE consists of several polymer chains that are all interacting with configurations that are randomly distributed. While it is a significant challenge to account for this randomness, we follow the eight-chain RVE-averaging approach of Arruda and Boyce (Fig. 2, [40]) in approximating the RVE in the undeformed state as composed of eight polymer chains connecting the center of a cube to each of the corners. The RVE then deforms under the action of the macroscopic deformation tensor $\boldsymbol{F}$, i.e., the chain end-to-end vectors are mapped by $\boldsymbol{F}$ from the undeformed to the deformed state (Fig. 3, [72]). An important element of Ref. [40] is that the RVE is oriented such that the cube is oriented along the principal directions of the stretch tensor $\boldsymbol{U}$, where $\boldsymbol{U}$ is the tensor square root of $\boldsymbol{F}$, and can be obtained through the polar decomposition $\boldsymbol{F} = \boldsymbol{RU}$ where $\boldsymbol{R} \in SO(3)$.

Given the mapping of the end-to-end vectors of the chains, the polymer field theory is then used to compute the partition function of the deformed state, from which we can find the free energy and stress. Following Ref. [59], we use the continuous Gaussian chain model for a single polymer chain. Next, we consider chain segments that interact pairwise in real space, and nonlocally in terms of position along the chain contour (Fig. 1), through a pairwise interaction potential of mean force; these are given by Dirac potentials to model excluded volume effects. Given the intersegment interaction and end-to-end vectors, the framework of polymer field theory enables us to compute, using the self-consistent scheme, the partition function, and consequently the free energy of the RVE. We notice that because the ends of the polymer chain are constrained by the macroscale deformation $\boldsymbol{F}$, this leads to a restricted ensemble. Further, nonlinear elasticity provides the Piola-Kirchoff stress tensor $\boldsymbol{P}$ as the energy-conjugate of $\boldsymbol{F}$, enabling us to compute the stress-deformation response of the polymer network.

Key results from the model are as follows. In the absence of excluded volume interactions, we find that the closed-form orientationally averaged elastic response matches with classical rubber elasticity [72]. Considering excluded volume interactions, closed-form solutions appear impossible, and we develop a three-dimensional (3D) finite element method (FEM) implementation to self-consistently solve the equations of the polymer field theory. We find that the linearized Poisson's ratio $\nu \simeq 0.4943$, which is very close to the incompressible limit $\nu \to 0.5$, without a phenomenological imposition of incompressibility, and that the elastic moduli are in line with typical polymer network gels. Further, despite the harmonic Gaussian chain as a starting point, there is an emergent strain-softening and strain-stiffening response that is characteristic of real polymer networks, driven by

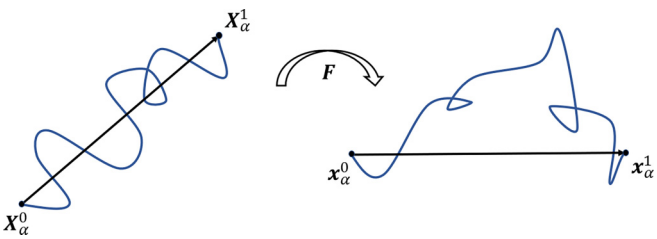

FIG. 3. The end-to-end vector in the undeformed state, $(\boldsymbol{X}^1_\alpha - \boldsymbol{X}^0_\alpha)$, is mapped by the deformation $\boldsymbol{F}$ to the end-to-end vector in the deformed state, $\boldsymbol{x}^1_\alpha - \boldsymbol{x}^0_\alpha$, i.e., $\boldsymbol{x}^1_\alpha - \boldsymbol{x}^0_\alpha = \boldsymbol{F}(\boldsymbol{X}^1_\alpha - \boldsymbol{X}^0_\alpha)$.

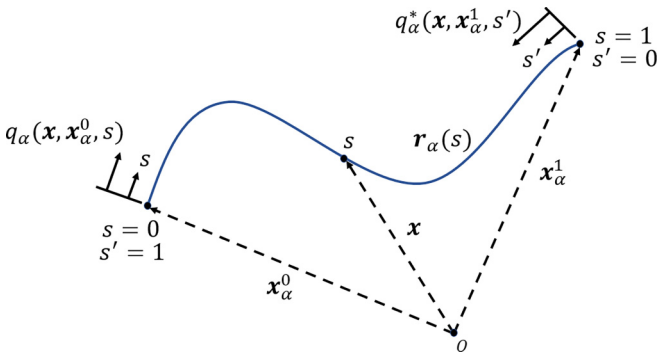

FIG. 4. Single polymer chain fixed at both ends.

the interplay between the excluded volume interactions and the entropy; it does not require chains with limiting extensibility, such as the inverse Langevin approximation, to model this behavior. Finally, we find the emergence of a deformation-sensitive localization instability at large values of the excluded volume parameter.

The structure of the paper is as follows. Section II formulates the model. Section III summarizes the finite element approach for the self-consistent solution. Section IV presents numerical results showing the predictions of the model.

II. MODEL FORMULATION

A. Deformation of a single polymer chain

We use the continuous Gaussian chain model for a single polymer chain [58]. In the undeformed state, the coarse-grained trajectory of the αth polymer chain is represented as a continuous 3D space curve $\boldsymbol{R}_\alpha(s)$, where s is the chain contour coordinate and varies along the chain contour, and is scaled such that $0 \leqslant s \leqslant 1$. The position vectors of the beginning and end points of the chain in the undeformed state are $\boldsymbol{X}^0_\alpha$ and $\boldsymbol{X}^1_\alpha$.

The chain is deformed under the deformation gradient $\boldsymbol{F}$. In the deformed state, $\boldsymbol{r}_\alpha(s)$ is a 3D curve that represents the coarse-grained trajectory of the αth chain, as shown in Fig. 4. The position vectors of the beginning and end of the chain in the deformed state are $\boldsymbol{x}^0_\alpha$ and $\boldsymbol{x}^1_\alpha$.

Following Ref. [72], we use that the chain end-to-end vector is mapped under the macroscale deformation $\boldsymbol{F}$:

$$\boldsymbol{x}^1_\alpha - \boldsymbol{x}^0_\alpha = \boldsymbol{F}\big(\boldsymbol{X}^1_\alpha - \boldsymbol{X}^0_\alpha\big). \tag{2.1}$$

We note that the affine deformation assumption depends strongly on the assumption that there are no entanglements [73–76].

1. Partition function and average segment density

Consider the αth chain that consists of N coarse-grained polymer segments each of length a, and under the influence of a field $w(\boldsymbol{x})$ that will be used to account for the excluded volume interactions [59]. From Ref. [58], the partition function, $Q_\alpha[w;\boldsymbol{F}]$, and the average segment density, $\langle\hat{\rho}_\alpha(\boldsymbol{x};\boldsymbol{F})\rangle$, are

$$Q_\alpha[w;\boldsymbol{F}] = \frac{1}{V}\int d\boldsymbol{x}\; q_\alpha\big(\boldsymbol{x}, \boldsymbol{x}^0_\alpha, s\big)\; q^*_\alpha\big(\boldsymbol{x}, \boldsymbol{x}^1_\alpha, 1-s\big), \tag{2.2}$$

$$\langle\hat{\rho}_\alpha(\boldsymbol{x};\boldsymbol{F})\rangle = \frac{1}{VQ_\alpha[w;\boldsymbol{F}]}\int_0^1 ds\; q_\alpha\big(\boldsymbol{x}, \boldsymbol{x}^0_\alpha, s\big)\; q^*_\alpha\big(\boldsymbol{x}, \boldsymbol{x}^1_\alpha, 1-s\big). \tag{2.3}$$

Here, $q_\alpha(\boldsymbol{x}, \boldsymbol{x}^0_\alpha, s)$ and $q^*_\alpha(\boldsymbol{x}, \boldsymbol{x}^1_\alpha, 1-s)$ are the partial partition functions for the two chain fragments, one from 0 to s and the other from 1 to s, respectively, as shown in Fig. 4.

$q_\alpha(\boldsymbol{x}, \boldsymbol{x}^0_\alpha, s)$ is obtained by solving the following PDE with the initial condition:

$$\frac{\partial q_\alpha\big(\boldsymbol{x}, \boldsymbol{x}^0_\alpha, s\big)}{\partial s} = \frac{a^2N}{6}\nabla^2 q_\alpha\big(\boldsymbol{x}, \boldsymbol{x}^0_\alpha, s\big) - w(\boldsymbol{x})q_\alpha\big(\boldsymbol{x}, \boldsymbol{x}^0_\alpha, s\big),$$
$$q_\alpha\big(\boldsymbol{x}, \boldsymbol{x}^0_\alpha, s\big)\big|_{s=0} = (aN^{1/2})^3\,\delta\big(\boldsymbol{x} - \boldsymbol{x}^0_\alpha\big). \tag{2.4}$$

Similarly, $q^*_\alpha(\boldsymbol{x}, \boldsymbol{x}^1_\alpha, s')$ is obtained by solving the same PDE as in (2.4), but with the initial condition corresponding to keeping the other end fixed:

$$\frac{\partial q^*_\alpha\big(\boldsymbol{x}, \boldsymbol{x}^1_\alpha, s'\big)}{\partial s'} = \frac{a^2N}{6}\nabla^2 q^*_\alpha\big(\boldsymbol{x}, \boldsymbol{x}^1_\alpha, s'\big) - w(\boldsymbol{x})q^*_\alpha\big(\boldsymbol{x}, \boldsymbol{x}^1_\alpha, s'\big),$$
$$q^*_\alpha\big(\boldsymbol{x}, \boldsymbol{x}^1_\alpha, s'\big)\big|_{s'=0} = (aN^{1/2})^3\,\delta\big(\boldsymbol{x} - \boldsymbol{x}^1_\alpha\big). \tag{2.5}$$

The initial conditions above correspond to the physical constraint that the beginning and end points of the αth chain are fixed at the given spatial positions $\boldsymbol{x}^0_\alpha$ and $\boldsymbol{x}^1_\alpha$, respectively.

2. Reduction to classical rubber elasticity

In the absence of excluded volume interactions, obtained by setting $w(\boldsymbol{x}) \equiv 0$, we can find closed-form solutions for q_α and q^*_α:

$$q_\alpha\big(\boldsymbol{x}, \boldsymbol{x}^0_\alpha, s\big) = \left(\frac{3}{2\pi s}\right)^{3/2}\exp\left(-\frac{3\big|\boldsymbol{x} - \boldsymbol{x}^0_\alpha\big|^2}{2a^2Ns}\right), \tag{2.6}$$

$$q^*_\alpha\big(\boldsymbol{x}, \boldsymbol{x}^1_\alpha, 1-s\big) = \left(\frac{3}{2\pi(1-s)}\right)^{3/2}\exp\left(-\frac{3\big|\boldsymbol{x} - \boldsymbol{x}^1_\alpha\big|^2}{2a^2N(1-s)}\right). \tag{2.7}$$

The partition function $Q_\alpha[w;\boldsymbol{F}]\big|_{w=0}$ in (2.2) evaluates to the classical Gaussian distribution in three dimensions:

$$Q_\alpha[w;\boldsymbol{F}]\big|_{w=0} \propto \left(\frac{3}{\sqrt{\pi}}\right)^3\left(\frac{a^2N}{6}\right)^{3/2} \times \exp\left(-\frac{3}{2a^2N}\big|\boldsymbol{x}^1_\alpha - \boldsymbol{x}^0_\alpha\big|^2\right). \tag{2.8}$$

Because the chains do not interact, the free energy of the αth polymer chain, H_α, is obtained from Q_α using $H_\alpha = -k_BT\log Q_\alpha$ to be:

$$H_\alpha[w;\boldsymbol{F}]\big|_{w=0} = \frac{1}{2}\left(\frac{3k_BT}{a^2N}\right)\big|\boldsymbol{F}\big(\boldsymbol{X}^1_\alpha - \boldsymbol{X}^0_\alpha\big)\big|^2 - \left(\frac{3k_BT}{2}\right). \tag{2.9}$$

To account for the fact that chains are randomly oriented, we next average $H_\alpha[w;\boldsymbol{F}]\big|_{w=0}$ over all possible orientations of the chain end-to-end vector by integrating (2.9) over all orientations. That is, keeping $\boldsymbol{F}$ fixed, we integrate $(\boldsymbol{X}_\alpha^1 - \boldsymbol{X}_\alpha^0)$ over the sphere of appropriate radius. The resulting expression for the orientationally averaged free energy, $H_\alpha^{\text{avg}}[w;\boldsymbol{F}]\big|_{w=0}$, is

$$H_\alpha^{\text{avg}}[w;\boldsymbol{F}]\big|_{w=0} = \frac{k_B T}{2}(\text{tr}(\boldsymbol{F}^T\boldsymbol{F}) - 3). \tag{2.10}$$

This result recovers the classical rubber elasticity result [72], also known as the incompressible neo-Hookean elastic strain energy.

B. Deformation of the polymer network

The pairwise excluded volume interactions are introduced through the field $w(\boldsymbol{x})$ following Ref. [59]. We introduce $\bar{u}(|\boldsymbol{x}-\boldsymbol{x}'|)$, which is the pairwise interaction potential of mean force for two segments located at spatial coordinates $\boldsymbol{x}$ and $\boldsymbol{x}'$. The corresponding partition function for the polymer network in the deformed state, $Z(\boldsymbol{F})$ in the field-theoretic setting is

$$Z(\boldsymbol{F}) \propto \int \mathrm{D}\rho \int \mathrm{D}w \, \exp\left(-\frac{H[w,\rho;\boldsymbol{F}]}{k_B T}\right), \tag{2.11}$$

where $H[w,\rho;\boldsymbol{F}]$ is the effective Hamiltonian of the polymer network, and has the expression:

$$\begin{aligned}\frac{H[w,\rho;\boldsymbol{F}]}{k_B T} = &-\int d\boldsymbol{x}\, w(\boldsymbol{x})\rho(\boldsymbol{x}) \\ &+ \frac{1}{2k_B T}\int d\boldsymbol{x}\int d\boldsymbol{x}'\, \rho(\boldsymbol{x})\,\bar{u}(|\boldsymbol{x}-\boldsymbol{x}'|)\,\rho(\boldsymbol{x}') \\ &- \log\left(Q_1[w;\boldsymbol{F}]\ldots Q_n[w;\boldsymbol{F}]\right).\end{aligned} \tag{2.12}$$

The auxiliary fields $w(\boldsymbol{x})$ and $\rho(\boldsymbol{x})$ are interpreted as the fluctuating chemical potential field generated internally because of the intersegment interactions and the fluctuating density of the polymer network, respectively [59]. $Q_\alpha[w;\boldsymbol{F}]$ is the partition function for the αth chain in the polymer network under the influence of $w(\boldsymbol{x})$, and is calculated using (2.2).

The first term in (2.12) is the energy of interaction between the density and the chemical potential. The second term is the intersegment interaction energy. The third term is the entropic contribution due to chain stretching. The total Helmholtz free energy of polymer network in the deformed state, $H(\boldsymbol{F})$, is evaluated from the partition function $Z(\boldsymbol{F})$ in (2.11) using:

$$H(\boldsymbol{F}) = -k_B T \log Z(\boldsymbol{F}). \tag{2.13}$$

In the deformed state, the average segment density of the polymer network, $\langle\hat{\rho}(\boldsymbol{x};\boldsymbol{F})\rangle$, is obtained as:

$$\begin{aligned}\langle\hat{\rho}(\boldsymbol{x};\boldsymbol{F})\rangle \propto \frac{1}{Z(\boldsymbol{F})}\int \mathrm{D}\rho\int \mathrm{D}w \Bigg[&\exp\left(\int d\boldsymbol{x}\, w(\boldsymbol{x})\rho(\boldsymbol{x}) - \frac{1}{2k_B T}\int d\boldsymbol{x}\int d\boldsymbol{x}'\rho(\boldsymbol{x})\bar{u}(|\boldsymbol{x}-\boldsymbol{x}'|)\rho(\boldsymbol{x}')\right) \\ &\times\left(\sum_{i=1}^{n}\left(\left(\int_0^1 ds\, q_i(\boldsymbol{x},\boldsymbol{x}_i^0,s)\, q_i^*(\boldsymbol{x},\boldsymbol{x}_i^1,1-s)\right)\prod_{\substack{k=1\\k\neq i}}^{n} Q_k[w;\boldsymbol{F}]\right)\right)\Bigg].\end{aligned} \tag{2.14}$$

C. Strain energy density of the polymer network

To obtain the continuum elastic response using nonlinear elasticity, we introduce the elastic energy density (per undeformed unit volume) $W(\boldsymbol{F})$ and treat the RVE as a continuum material point. This allows us to connect the total free energy $H(\boldsymbol{F})$ evaluated for the RVE to $W(\boldsymbol{F})$ at the corresponding spatial location:

$$W(\boldsymbol{F}) = \frac{H(\boldsymbol{F})}{V}, \tag{2.15}$$

where V is the volume of the RVE in the undeformed state.

We can then find the Piola-Kirchhoff stress tensor $\boldsymbol{P}$ and the fourth-order elasticity tensor $\mathbb{C} = [C_{ijkl}]$ using:

$$\boldsymbol{P} = \frac{\partial W}{\partial \boldsymbol{F}}, \tag{2.16}$$

$$C_{ijkl} = \left.\frac{\partial^2 W}{\partial F_{ij}\partial F_{kl}}\right|_{\boldsymbol{F}=\boldsymbol{I}}, \tag{2.17}$$

where $\boldsymbol{I}$ is the second-order identity tensor.

Applying (2.16), and substituting from (2.11), (2.12), (2.13), (2.15), we have:

$$\begin{aligned}\boldsymbol{P} = \frac{\partial W}{\partial \boldsymbol{F}} &= -\frac{k_B T}{V}\frac{1}{Z(\boldsymbol{F})}\frac{\partial Z(\boldsymbol{F})}{\partial \boldsymbol{F}} = -\frac{k_B T}{V}\frac{1}{Z(\boldsymbol{F})}\int \mathrm{D}\rho\int \mathrm{D}w\exp\left(-\frac{H[w,\rho;\boldsymbol{F}]}{k_B T}\right)\frac{\partial H[w,\rho;\boldsymbol{F}]}{\partial \boldsymbol{F}}\left(-\frac{1}{k_B T}\right) \\ &= -\frac{k_B T}{V}\frac{1}{Z(\boldsymbol{F})}\int \mathrm{D}\rho\int \mathrm{D}w\exp\left(-\frac{H[w,\rho;\boldsymbol{F}]}{k_B T}\right)\sum_{\alpha=1}^{n}\frac{\partial}{\partial \boldsymbol{F}}\log Q_\alpha[w;\boldsymbol{F}].\end{aligned} \tag{2.18}$$

Then, defining the stress operator for the αth chain, $\hat{\boldsymbol{P}}_\alpha$, as:

$$\hat{\boldsymbol{P}}_\alpha := -\frac{\partial}{\partial \boldsymbol{F}} \log Q_\alpha[w;\boldsymbol{F}], \tag{2.19}$$

we can write $\boldsymbol{P}$ as the statistical average ([58], Sec. 4.1.3] of $\hat{\boldsymbol{P}}_\alpha$:

$$\boldsymbol{P} = \frac{k_B T}{V}\left(\frac{1}{Z(\boldsymbol{F})}\int \mathrm{D}\rho \int \mathrm{D}w \exp\left(-\frac{H[w,\rho;\boldsymbol{F}]}{k_B T}\right)\sum_{\alpha=1}^{n}\hat{\boldsymbol{P}}_\alpha\right)$$
$$= \frac{k_B T}{V}\sum_{\alpha=1}^{n}\langle \hat{\boldsymbol{P}}_\alpha\rangle. \tag{2.20}$$

D. Mean-field assumption

The functional integration over the fields w and ρ in (2.11) and (2.14) makes it expensive to evaluate $H(\boldsymbol{F})$ and $\langle\hat{\rho}(\boldsymbol{x};\boldsymbol{F})\rangle$. Therefore, it is common to use a mean-field assumption to simplify the functional integration in the expression for $Z(\boldsymbol{F})$ in (2.11) [58]. This assumption implies that functional integration over the fields w and ρ is dominated by the mean fields $\bar{w}$ and $\bar{\rho}$, respectively. The mean fields $\bar{w}$ and $\bar{\rho}$ are obtained by requiring the effective Hamiltonian $H[w,\rho;\boldsymbol{F}]$ in (2.12) to be stationary with respect to variations in $w(\boldsymbol{x})$ and $\rho(\boldsymbol{x})$. This gives the self-consistent mean-field conditions:

$$\left.\frac{\delta H[w,\rho;\boldsymbol{F}]}{\delta w}\right|_{w=\bar{w}} = 0, \tag{2.21}$$

$$\left.\frac{\delta H[w,\rho;\boldsymbol{F}]}{\delta \rho}\right|_{\rho=\bar{\rho}} = 0. \tag{2.22}$$

Using the mean-field assumption, $Z(\boldsymbol{F})$ in (2.11) simplifies to:

$$Z(\boldsymbol{F}) \approx \exp\left(-\frac{H[\bar{w},\bar{\rho};\boldsymbol{F}]}{k_B T}\right), \tag{2.23}$$

where, $H[\bar{w},\bar{\rho};\boldsymbol{F}]$ is the effective Hamiltonian in (2.12) evaluated using the mean fields $\bar{w}$ and $\bar{\rho}$. Using (2.13) and (2.23), the total free energy of polymer network, $H(\boldsymbol{F})$ under the mean-field assumption is

$$\frac{H(\boldsymbol{F})}{k_B T} = -\int d\boldsymbol{x}\, \bar{w}(\boldsymbol{x})\bar{\rho}(\boldsymbol{x}) + \frac{1}{2k_B T}\int d\boldsymbol{x}\int d\boldsymbol{x}'\, \bar{\rho}(\boldsymbol{x})\,\bar{u}(|\boldsymbol{x}-\boldsymbol{x}'|)\,\bar{\rho}(\boldsymbol{x}') - \log\left(Q_1[\bar{w};\boldsymbol{F}]\cdots Q_n[\bar{w};\boldsymbol{F}]\right). \tag{2.24}$$

Further, the average segment density, $\langle\hat{\rho}(\boldsymbol{x};\boldsymbol{F})\rangle$, in (2.14) simplifies to:

$$\langle\hat{\rho}(\boldsymbol{x};\boldsymbol{F})\rangle \approx \left.\sum_{\alpha=1}^{n}\langle\hat{\rho}_\alpha(\boldsymbol{x};\boldsymbol{F})\rangle\right|_{w=\bar{w}}, \tag{2.25}$$

where $\langle\hat{\rho}_\alpha(\boldsymbol{x};\boldsymbol{F})\rangle$ is the average segment density of the αth chain in the polymer network, obtained using (2.3).

E. Excluded volume interaction

Polymer segments in the network are considered to interact with each other according to a pairwise interaction potential of mean force $\bar{u}$ whose physical origin is due to excluded volume effects. We account for the excluded volume effects by modeling a pairwise intersegment interaction using a simple Dirac delta potential of mean force [57,77]:

$$\bar{u}(|\boldsymbol{x}-\boldsymbol{x}'|) = k_B T\; u_0\; \delta(|\boldsymbol{x}-\boldsymbol{x}'|), \tag{2.26}$$

where u_0 is the excluded volume parameter. This form of intersegment interaction potential assumes the presence of a solvent in the polymer network system with low density [49,57]. The solvent mediates the interactions among polymer segments. For $u_0 > 0$, implying repulsion between the segments, the excluded volume potential $\bar{u}$ in (2.26) is positive-definite and has an inverse; following [58], this simplifies the field theory equations in (2.11) to:

$$Z(\boldsymbol{F}) \propto \int \mathrm{D}w \exp\left(-\frac{H[w;\boldsymbol{F}]}{k_B T}\right), \tag{2.27}$$

where $H[w;\boldsymbol{F}]$ is the effective Hamiltonian of polymer network in the simplified field theory:

$$\frac{H[w;\boldsymbol{F}]}{k_B T} = \frac{1}{2u_0}\int d\boldsymbol{x}\,(w(\boldsymbol{x}))^2 - \log(Q_1[w;\boldsymbol{F}]\cdots Q_n[w;\boldsymbol{F}]). \tag{2.28}$$

Equations (2.27) and (2.28) present the simplified field theory for the deformation of polymer network that is used in this work. The partition function in (2.27) is evaluated using the mean-field assumption as:

$$Z(\boldsymbol{F}) \approx \exp\left(-\frac{H[\bar{w};\boldsymbol{F}]}{k_B T}\right), \tag{2.29}$$

where $H[\bar{w};\boldsymbol{F}]$ is the effective Hamiltonian in (2.28) evaluated using the mean field $\bar{w}$. The mean field $\bar{w}$ is obtained by solving the stationarity condition for the effective Hamiltonian $H[w;\boldsymbol{F}]$:

$$\left.\frac{\delta H[w;\boldsymbol{F}]}{\delta w}\right|_{w=\bar{w}} = 0. \tag{2.30}$$

For the assumed form of the excluded volume interaction potential as in (2.26), there is alternatively an expression for the average segment density [58]:

$$\langle\hat{\rho}(\boldsymbol{x};\boldsymbol{F})\rangle = \frac{1}{u_0}\langle w(\boldsymbol{x})\rangle = \frac{\bar{w}(\boldsymbol{x})}{u_0}, \tag{2.31}$$

where $\langle w(\boldsymbol{x})\rangle$ is the statistical average of the fluctuating field $w(\boldsymbol{x})$, and we use that under the mean-field assumption $\langle w(\boldsymbol{x})\rangle = \bar{w}(\boldsymbol{x})$. Finally, using (2.29) and (2.13), we obtain the total free energy of polymer network, $H(\boldsymbol{F})$ for the simplified field theory as:

$$\frac{H(\boldsymbol{F})}{k_B T} = \frac{1}{2u_0}\int d\boldsymbol{x}(\bar{w}(\boldsymbol{x}))^2 - \log(Q_1[\bar{w};\boldsymbol{F}]\cdots Q_n[\bar{w};\boldsymbol{F}]), \tag{2.32}$$

where $\bar{w}(\boldsymbol{x})$ is obtained by self-consistently solving (2.31) and the mean-field condition in (2.30).

F. Representative volume element averaging: Eight-chain model

A typical polymer network consists of a large number of cross-linked polymer chains (Fig. 2) with random orientations at each continuum point, and is very challenging to directly

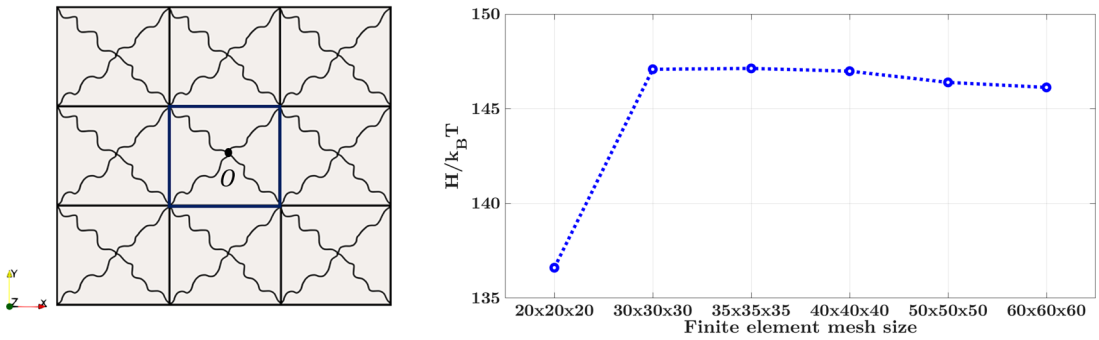

(a) (b)

FIG. 5. (a) Front view schematic of a bigger physical domain in three dimensions that consists of 27 RVEs, each with eight chains. The central eight-chain RVE (highlighted) is used for the free-energy calculation. (b) The convergence of the energy as the mesh is refined, shown by plotting the free energy of a single chain without external field as a function of mesh size. The converged mesh size of 35^3 elements is used for the numerical computations. Note that the saddle point nature of the problem can lead to nonmonotonic convergence.

solve. To simplify this problem, we adopt the eight-chain model for the RVE [40]. The 3D RVE is assumed to be a cube in the undeformed configuration, with eight chains running between the center and each of the corners. The cube is assumed to be oriented along the principal directions of the macroscale right stretch tensor $\boldsymbol{U}$, where $\boldsymbol{U}$ is the tensor square root of the deformation $\boldsymbol{F}$ or alternatively is the positive-definite part of the right polar decomposition of $\boldsymbol{F}$.

We assume that each chain begins ($s = 0$) at the center of the cube, which is also taken to be the origin, and the chains terminate ($s = 1$) at the corners. Denoting the terminating point of the chains in the undeformed and deformed state, respectively, by $\boldsymbol{X}_1^1, \ldots \boldsymbol{X}_8^1$ and $\boldsymbol{x}_1^1, \ldots \boldsymbol{x}_8^1$, the relation between the end-to-end vectors in the undeformed and deformed configurations from (2.1) is

$$\boldsymbol{x}_\alpha^1 = \boldsymbol{F}\, \boldsymbol{X}_\alpha^1, \quad \alpha = 1, \ldots 8. \tag{2.33}$$

For a given value of $\boldsymbol{F}$, the right stretch tensor $\boldsymbol{U}$ is used to orient the cube, and the equation above provides the initial conditions for the partial partition functions q and q^* of each chain in (2.4) and (2.5).

III. NUMERICAL METHOD

Since the model with excluded volume interactions is not amenable to simple closed-form solutions, we turn to numerical solutions. The goal is to evaluate the total free energy $H(\boldsymbol{F})$ and average segment density $\langle \hat{\rho}(\boldsymbol{x}; \boldsymbol{F}) \rangle$. Our numerical method has the following steps:

(1) We first generate an initial field $w(\boldsymbol{x}) = w^0(\boldsymbol{x})$. The initial guess can be based on heuristics when possible.

(2) We next solve for the average segment density $\langle \hat{\rho}(\boldsymbol{x}; \boldsymbol{F}) \rangle$, using q and q^* obtained by solving (2.4) and (2.5) with the given $w(\boldsymbol{x})$, and the total free energy $H(\boldsymbol{F})$ using (2.30).

(3) The field w is updated using (2.31) as $w(\boldsymbol{x}) = u_0 \langle \hat{\rho}(\boldsymbol{x}; \boldsymbol{F}) \rangle$.

(4) In turn, we update $\langle \hat{\rho}(\boldsymbol{x}; \boldsymbol{F}) \rangle$ and $H(\boldsymbol{F})$ as above.

This iteration continues until we reach convergence, which we define as a relative change in the total free energy of less than 0.1%.

For the solution of q and q^* in (2.4) and (2.5), we use the finite element method (FEM) in the open-source FEniCS framework [78]. The spatial domain is discretized using first-order Lagrange family finite elements. The integration along the chain with respect to s in (2.4) and in (2.5) is performed using the implicit Crank-Nicholson finite difference method with 100 steps for $s \in (0, 1)$. We test convergence of the FEM discretization as in Fig. 5(b).

While the RVE averaging nominally requires only eight chains, these chains interact not only with each other, but also with other chains that are not contained in the RVE. To account for this, we use periodic images of the RVE; we find that one image on each face of the cubic RVE is sufficient, giving us 27 cubes over which we must perform various integrations; Fig. 5(a) shows a schematic projection of this in two dimensions, where the highlighted central RVE is used for the energy calculations. When the deformation is applied, the image RVEs are deformed following the central RVE. Similarly, $w(\boldsymbol{x})$ is defined over the larger cluster of RVEs for performing, but need only be solved on the central RVE using periodicity.

IV. ELASTIC RESPONSE WITH EXCLUDED VOLUME INTERACTIONS

In the calculations reported here, we use the following model parameters: total chain contour length $L = 0.12$ μm, number of polymer segments in single chain $N = 100$, excluded volume parameter $u_0 = 0.005\ v_{\text{seg}}$ where $v_{\text{seg}} = a^3$ is the volume of an individual monomer segment, and temperature $T = 303$ K. This choice of u_0 gives an excluded cube with side $0.17a$, and corresponds to the Flory-Huggins interaction parameter $\chi = 0.4975$, using $u_0 = (1 - 2\chi) v_{\text{seg}}$. This characterizes a good solvent that is very close to the Θ point [54,58,79,80].

For the numerical calculations, larger values of u_0 in three dimensions require an excessively fine mesh to converge; however, the calculations described below qualitatively agree with 2D calculations, where much larger values of u_0 can be used, and with a few representative 3D calculations that were conducted with a larger value of u_0 and a very fine mesh.

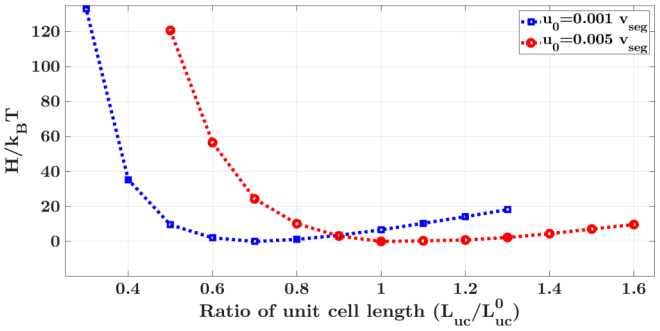

FIG. 6. The total free energy as a function of the relative stretch for $u_0 = 0.001\ v_{\text{seg}}$ and $u_0 = 0.005\ v_{\text{seg}}$.

A. Identifying the stress-free free-energy minimizing state

We first note that without excluded volume effects, all models based on the Gaussian chain approximation would predict that the polymer network shrinks to a point ($\boldsymbol{F} = \boldsymbol{0}$) because that would maximize the configurational entropy of the chain. Therefore, as we add excluded volume effects, we find that the equilibrium, stress-free or minimum energy, volume of the polymer network RVE increases. Specifically, the equilibrium state is achieved as a balance between the competing effects of entropic shrinkage and excluded volume repulsion between monomers; Refs. [81,82] examine related issues in greater depth.

We denote the initial side of the cubic RVE by $L^0_{uc} := 2aN^{1/2}/\sqrt{3}$, where $aN^{1/2}$ is the RMS average diameter of an unconstrained chain, and the prefactor accounts for the geometry of the chain aligned along the diagonal of the RVE. However, we emphasize that this is not the free-energy minimizing state, i.e., it is not stress free, in the presence of excluded volume interactions. To this initial state, we apply a deformation of the form $\boldsymbol{F} = \lambda \boldsymbol{I}$, and compute the free energy for various values of λ. Figure 6 shows the total free energy H as a function of $\lambda = L_{uc}/L^0_{uc}$ for $u_0 = 0.001\ v_{\text{seg}}$ and $u_0 = 0.005\ v_{\text{seg}}$. We find that the stress-free stretches, i.e., the free-energy minimizing stretches, for $u_0 = 0.001\ v_{\text{seg}}$ and $u_0 = 0.005\ v_{\text{seg}}$ are respectively at $\lambda = 0.7$ and $\lambda = 1$, respectively. The large increase in the equilibrium volume of the polymer network system with an increase in the excluded volume parameter u_0 is consistent with the phenomena of equilibrium swelling for polymeric gels [83–86].

In all of the subsequent calculations discussed below, we set the undeformed state to correspond to the free-energy minimizing stress-free state.

B. Volumetric and shear response, and near incompressibility

We use the strain energy density $W(\boldsymbol{F})$ to obtain the mesoscale elastic response using nonlinear elasticity; specifically, (2.16) and (2.17) are used to obtain the stress-stretch response and the elastic moduli, respectively. We assume below that the network can be treated as approximately isotropic despite the eight-chain model.

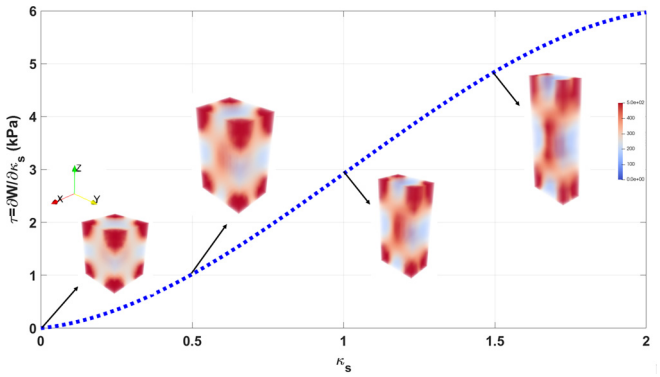

FIG. 7. Shear stress τ vs. shear strain κ_s in simple shear. The segment density for the RVE at various stretches are shown in the insets. We notice that the chains have higher concentrations at the ends when the deformation is small, but are more uniformly distributed as the deformation increases. Note that the RVE itself does not appear to be sheared because the chain-averaging approach aligns the averaging RVE along the principal directions that correspond to the maximum and minimum elongation directions (Fig. 2).

To obtain the bulk and shear moduli, we impose deformations of the form:

$$\boldsymbol{F}_v = \begin{bmatrix} \lambda & 0 & 0 \\ 0 & \lambda & 0 \\ 0 & 0 & \lambda \end{bmatrix}, \quad \boldsymbol{F}_s = \begin{bmatrix} 1 & \kappa_s & 0 \\ 0 & 1 & 0 \\ 0 & 0 & 1 \end{bmatrix}. \tag{4.1}$$

The bulk and shear moduli, K and G, respectively, can be computed using:

$$K = \frac{1}{9}\frac{\partial^2 W}{\partial \lambda^2}\bigg|_{\lambda\approx 1}, \quad G = \frac{\partial^2 W}{\partial \kappa_s^2}\bigg|_{\kappa_s\approx 0}. \tag{4.2}$$

We find $K = 52.06\,\text{kPa}$ and $G = 0.60\,\text{kPa}$. Using isotropic linearized elasticity, this gives the Poisson's ratio $\nu = \frac{3K-2G}{6K+2G} = 0.4943$ and the elastic modulus $E = \frac{9KG}{3K+G} = 1.79\,\text{kPa}$. These elastic moduli are consistent with polymer network gels [22,87–94]. We highlight that K is 2 orders of magnitude larger than G, and ν is very close to the incompressible limit of 0.5.

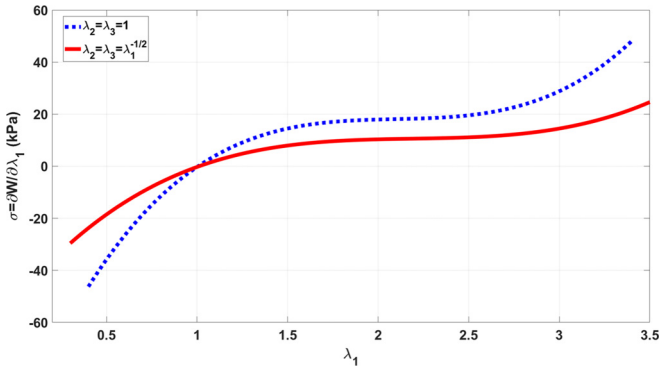

FIG. 8. The stress-strain curves for the constrained and volume-preserving extensional loadings. We notice that the stresses and the tangent moduli are both significantly larger when the system is constrained to undergo deformations that do not preserve the volume.

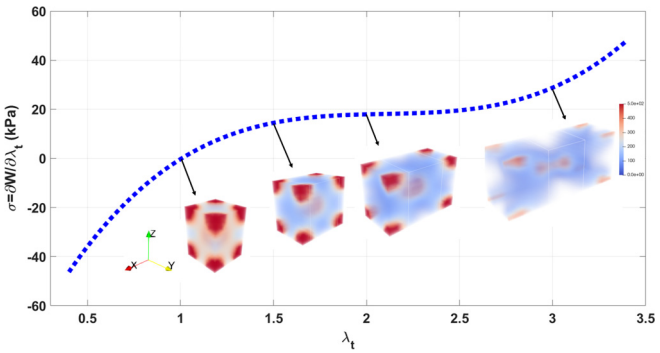

FIG. 9. Extensional stress σ vs. extensional stretch λ_t for the constrained case from Fig. 8. The segment density for the RVE at various stretches are shown in the insets. As with shearing, we notice that the chains have higher concentrations at the ends when the deformation is small, but are more uniformly distributed as the deformation increases.

We next examine the shear stress vs. shear strain curve. In principle, the shear stress can be computed using $\tau = \frac{\partial W}{\partial \kappa_s}$. To avoid a lot of noise from numerical differentiation, we fit W by a polynomial and then differentiate the polynomial to obtain the curve shown in Fig. 7.

C. Extensional response: Emergent strain softening and strain stiffening

We next examine extensional loading where the deformation has the form:

$$\boldsymbol{F}_e = \begin{bmatrix} \lambda_1 & 0 & 0 \\ 0 & \lambda_2 & 0 \\ 0 & 0 & \lambda_3 \end{bmatrix}. \tag{4.3}$$

Here, we consider λ_1 as the extensional stretch of interest. We make two different choices for the transverse stretches λ_2 and λ_3: the constrained case where they are constrained such that $\lambda_2 = \lambda_3 = 1$; and the volume-preserving case where they are set to be volume preserving such that $\lambda_2 = \lambda_3 = \lambda_1^{-\frac{1}{2}}$. Note that the second case is approximately equivalent to having no transverse stress. To obtain the extensional stress, we use $\sigma = \frac{\partial W}{\partial \lambda_1}$. Figure 8 compares the stress-strain response of these cases. We notice that the constrained case has significantly higher stresses and tangent moduli. Figure 9 shows the evolution of the chain density with stretch for the constrained case.

From Figs. 8 and 9, we notice that both cases show a pronounced strain-softening and strain-stiffening behavior that is characteristic of many real polymer networks such as polymeric gels. However, Gaussian chains do not show such behavior, and it is typical to use chains with limiting extensibility, such as the inverse Langevin approximation, to model this behavior. Here, we find that it is a consequence of the competition between the excluded volume parameter and the entropy. Figure 10 shows the decomposition of the free energy W into entropic W_{entropic} and excluded volume interaction $W_{\text{interaction}}$ contributions. We observe that the excluded volume contribution is less than the entropic contribution in both cases. Further, we notice that W_{entropic} monotonically increases with $\lambda_1 > 1$, and is consistent with the stretching of the Gaussian polymer chains; however, $W_{\text{interaction}}$ monotonically decreases with $\lambda_1 > 1$, and is consistent with the chains being more oriented, and hence having fewer excluded volume interactions. We notice that in the approximate range $1.5 < \lambda_1 < 2.5$ where we see strain softening, the decrease in the excluded volume interaction is faster than the rise in the entropic contribution, causing softening. For $\lambda_1 > 3$, we have the opposite trend in that the entropy increases faster than the decrease in the excluded volume interaction, causing stiffening. In summary, strain softening occurs because of the initial decrease in excluded volume interactions, and subsequent strain stiffening occurs because of the later increase in entropic effects.

D. Effect of chain length

Figure 11 shows the effect of chain contour length on the elastic moduli of the polymer network. The chain contour length L is varied from 0.01 μm–0.3 μm while keeping N fixed. We observe that both the elastic modulus E and the shear modulus G decrease with increased chain contour length. An increase in chain contour length corresponds to an increase in the average molecular weight (M_c) between the cross links, and these results are consistent with experiments

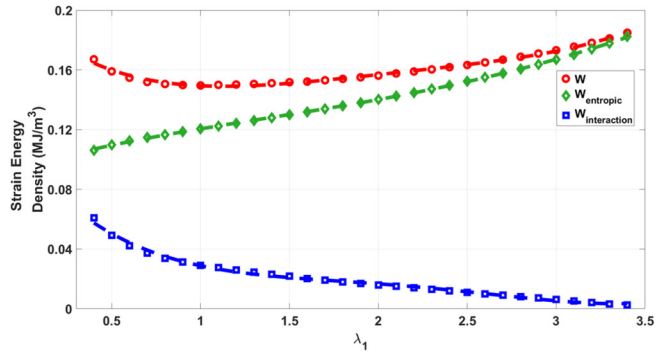

(a) Free energy density W vs stretch λ_1, with $\lambda_2 = \lambda_3 = 1$

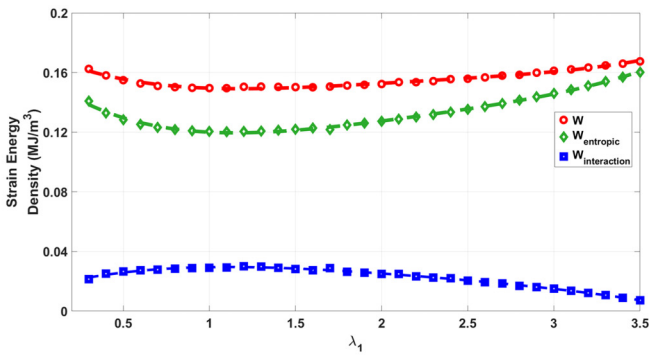

(b) Free energy density W vs stretch λ_1 with $\lambda_2 = \lambda_3 = \lambda_1^{-1/2}$

FIG. 10. The free energy W is decomposed into entropic W_{entropic} and excluded volume interaction $W_{\text{interaction}}$ contributions for the constrained and volume-preserving cases. The symbols show the simulation results, and the lines show best fits that are differentiated to obtain stress-strain curves.

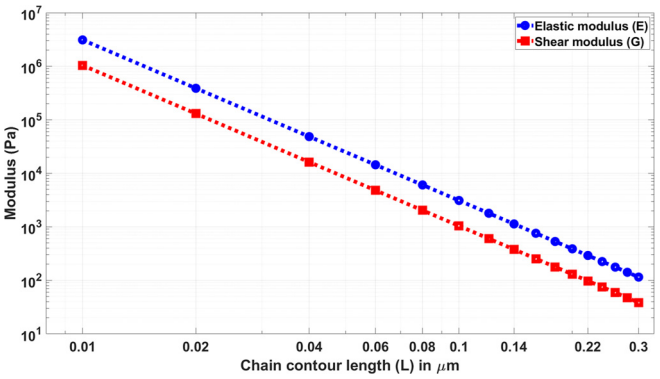

FIG. 11. Elastic and shear moduli as a function of chain contour length; as expected from polymer theory, these scale as a^{-3} [103].

that show that an increase in M_c corresponds to a decrease in the elastic moduli [95,96]. The range of elastic and shear moduli obtained using the model by varying chain contour length is consistent with the experimental values for polymer network soft matter such as elastomers and polymeric gels [22,87–94,97–102].

E. Interactions between deformation and an excluded volume instability

We next examine an instability driven by the increase in the excluded volume parameter. For computational feasibility, because we aim to numerically confirm that the instability is sharp by a large number of calculations near the instability, we focus on 2D systems; however, a few representative calculations suggest that 3D is qualitatively similar. Because it is in two dimensions, the undeformed RVE is a square with four chains.

Figure 12 presents the average segment density field for various equibiaxial stretches and various excluded volume parameter values. For a fixed RVE stretch of $L_{uc}/L^0_{uc} = 1$, where $L^0_{uc} = \sqrt{2}\ aN^{1/2}$ in two dimensions, we observe an instability at $u_0 \approx 0.7\ v_{\rm seg}$ ($v_{\rm seg} = a^2$ in two dimensions), leading to the localization of chains. Physically, the chains strongly repel each other and hence are highly restricted in the volume available. The instability is symmetry breaking, in that the originally square-symmetric chain configuration transitions to localize either vertically or horizontally from the original square symmetry; in our numerical simulations, we find that these occur essentially randomly due to numerical noise. As noted above, the instability is a sharp transition.

We examine the effect of an imposed equibiaxial stretch by setting L_{uc}/L^0_{uc} to 1.5 and 2, respectively. We notice that the critical values of u_0 for the instability are, respectively, $u_0 \approx 0.8\ v_{\rm seg}$ and $u_0 \approx 1.2\ v_{\rm seg}$. This coupling between the deformation and chain localization suggests new routes to obtain patterning in polymer networks.

V. DISCUSSION

We have used the statistical field theory of polymers in combination with the eight-chain network averaging approach to study the mechanical response of polymer networks. The framework of polymer field theory provides a physics-based approach to accounting for excluded volume interactions, which are imposed phenomenologically in micromechanical models. In the absence of excluded volume interactions, we find that that the closed-form orientationally averaged elastic response matches with the classical rubber elasticity [72].

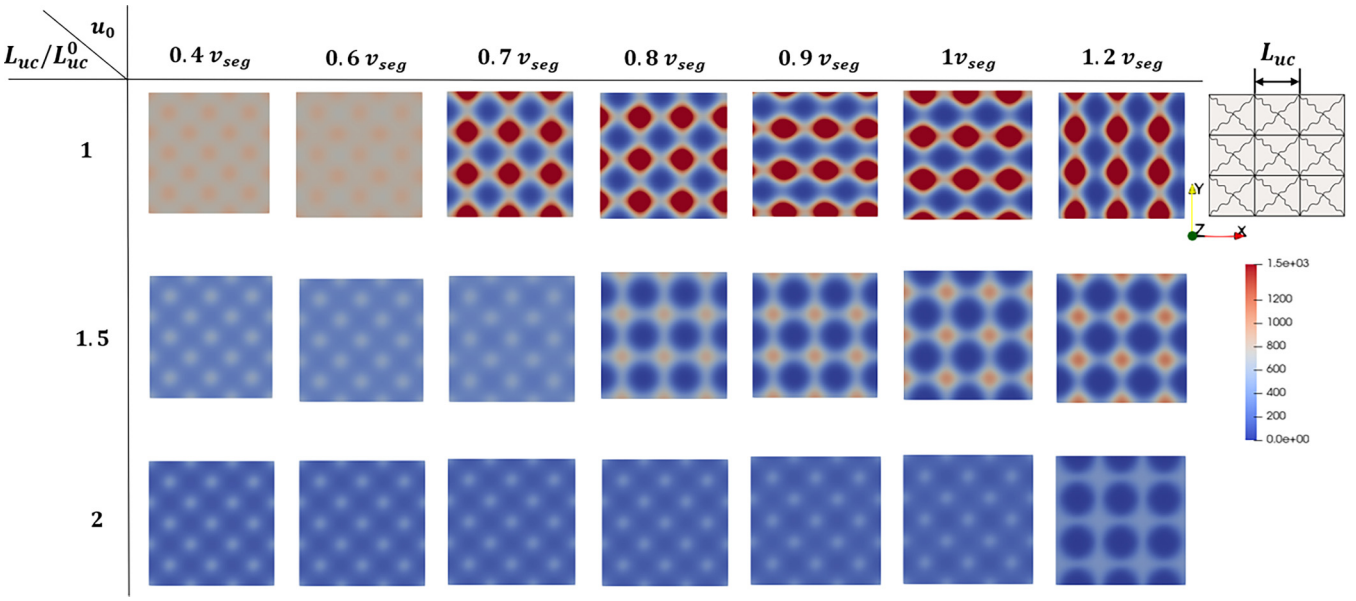

FIG. 12. Excluded volume-driven instability observed in two dimensions, and the effect of equi-biaxial deformation. Each subfigure shows the average segment density plotted over 9 RVEs, with each subfigure corresponding to different values of biaxial stretch L_{uc}/L^0_{uc} and u_0. The instability corresponds to a sharp transition in the chain configuration: it goes from being fairly uniform away from the cross linking point to being concentrated along the horizontal and vertical directions. As the stretch increases, the critical value of the excluded volume parameter at which the instability occurs also increases.

With excluded volume effects, self-consistent numerical solutions using finite elements find that the predicted elastic moduli are in line with typical polymer network gels; particularly, the linearized Poisson's ratio $\nu \simeq 0.4943$, which is very close to the incompressible limit $\nu \to 0.5$, without a phenomenological imposition of incompressibility. Though the equilibrium state depends on the value of u_0, the incompressible behavior is independent of the specific value of u_0 for the values studied here. This can be physically understood by considering that ν is computed around the equilibrium stress-free state. Due to entropic effects, the chains tend to reduce their end-to-end distance and would collapse to a point, while the excluded volume effects prevent the chains from collapsing completely. The equilibrium state is achieved when these opposing effects balance out. Around this equilibrium state, we find $\nu \simeq 0.5$, which reflects the role of the solvent in preventing further reduction in volume. Despite the seeming presence of voids or open space in the density fields, the chains are constrained due to the excluded volume interactions; the voids will be occupied by the solvent, which makes the system close to incompressible since the solvent cannot leave the polymer network upon deformation. This is consistent with the results of Ref. [104], wherein it was found that $\nu \simeq 0.5$ at short times when the solvent has not had time to diffuse out of the polymer network; at longer times, the solvent diffuses out and the long-time equilibrium value of ν depends on the shear modulus. While we have not considered this time-dependent behavior here, it is related to similar effects in poromechanics, namely the Terzaghi and Mandel model problems, wherein the stress response is closely tied to the drainage of the pore fluid [105–109].

Another interesting finding is that, despite the harmonic Gaussian chain as a starting point, there is an emergent strain-softening and strain-stiffening response that is characteristic of real polymer network gels, driven by the interplay between the excluded volume interactions and the entropy; it does not require chains with limiting extensibility, such as the inverse Langevin approximation, to model this behavior. We also we find the emergence of a deformation-sensitive localization instability at large values of the excluded volume parameter.

A natural question for the future is to examine the interplay between chain-scale instabilities such as microbuckling [110–112] and the network-scale instabilities observed here. We highlight, however, that these examples of instabilities are in fibrous networks, and it is possible that such instabilities occur here because of the regular network structure that has been assumed and will not appear in random networks. An important challenge, however, is that the isolated harmonic Gaussian chain does not display buckling or other instabilities; other nonlinear chain models are required to capture this behavior. Further, as noted in Ref. [8], electrical field interactions provide an effective compressive stiffness, and can induce new types of instabilities [12]. Incorporating chain models that go beyond the Gaussian approximation in polymer field theory is an interesting theoretical question. Along similar lines, while we capture strain stiffening and strain softening without the use of a chain model with limiting extensibility, such as the inverse Langevin model, it would be interesting to incorporate such models in polymer field theory to enable studying the interplay between entropic, excluded volume, and limited extensibility effects.

The concept of chain topology or entanglement is an important aspect that is not taken into consideration in this study. As highlighted in Refs. [73,74], these effects can play a significant role in the response of polymer networks. The mean-field framework employed in this study is unable to account for such effects directly. However, our inclusion of excluded volume effects provides some insight into the effects of entanglement. Additionally, we have observed that even without accounting for entanglements, excluded volume effects give rise to many interesting physical characteristics that are relevant to the response of real polymer networks. It should be noted that while entanglements are crucial for large deformation response, the linearized properties such as the Poisson's ratio are expected to be relatively unaltered.

A version of the code developed for this work is available online [113].

ACKNOWLEDGMENTS

We thank Carlos Garcia Cervera for useful discussions; NSF XSEDE for computing resources provided by the Pittsburgh Supercomputing Center; AFRL for hosting visits by Kaushik Dayal; NSF (DMREF 1921857, DMS 2108784), ONR (N00014-18-1-2528), BSF (2018183), and AFOSR (MURI FA9550-18-1-0095) for financial support; and the anonymous reviewers for comments that improved the paper significantly.

[1] Q. Deng, L. Liu, and P. Sharma, Electrets in soft materials: Nonlinearity, size effects, and giant electromechanical coupling, Phys. Rev. E **90**, 012603 (2014).

[2] L. Chen, X. Yang, B. Wang, S. Yang, K. Dayal, and P. Sharma, The interplay between symmetry-breaking and symmetry-preserving bifurcations in soft dielectric films and the emergence of giant electro-actuation, Extreme Mech. Lett. **43**, 101151 (2021).

[3] F. Ahmadpoor and P. Sharma, Flexoelectricity in two-dimensional crystalline and biological membranes, Nanoscale **7**, 16555 (2015).

[4] O. V. Kim, X. Liang, R. I. Litvinov, J. W. Weisel, M. S. Alber, and P. K. Purohit, Foam-like compression behavior of fibrin networks, Biomech. Model. Mechanobiol. **15**, 213 (2016).

[5] A. E. X. Brown, R. I. Litvinov, D. E. Discher, P. K. Purohit, and J. W. Weisel, Multiscale mechanics of fibrin polymer: gel stretching with protein unfolding and loss of water, Science **325**, 741 (2009).

[6] T. Su and P. K. Purohit, Semiflexible filament networks viewed as fluctuating beam-frames, Soft Matter **8**, 4664 (2012).

[7] M. Grasinger and K. Dayal, Architected elastomer networks for optimal electromechanical response, J. Mech. Phys. Solids **146**, 104171 (2021).

[8] M. Grasinger, C. Majidi, and K. Dayal, Nonlinear statistical mechanics drives intrinsic electrostriction and volumetric torque in polymer networks, Phys. Rev. E **103**, 042504 (2021).

[9] M. Grasinger and K. Dayal, Statistical mechanical analysis of the electromechanical coupling in an electrically-responsive polymer chain, Soft Matter **16**, 6265 (2020).

[10] N. Cohen, K. Dayal, and G. deBotton, Electroelasticity of polymer networks, J. Mech. Phys. Solids **92**, 105 (2016).

[11] F. Darbaniyan, K. Dayal, L. Liu, and P. Sharma, Designing soft pyroelectric and electrocaloric materials using electrets, Soft Matter **15**, 262 (2019).

[12] M. Grasinger, K. Mozaffari, and P. Sharma, Flexoelectricity in soft elastomers and the molecular mechanisms underpinning the design and emergence of giant flexoelectricity, Proc. Natl. Acad. Sci. USA **118**, e2102477118 (2021).

[13] M. Grasinger, Group action Markov chain Monte carlo for accelerated sampling of energy landscapes with discrete symmetries and energy barriers, arXiv:2205.00028.

[14] E. J. Markvicka, M. D. Bartlett, X. Huang, and C. Majidi, An autonomously electrically self-healing liquid metal–elastomer composite for robust soft-matter robotics and electronics, Nat. Mater. **17**, 618 (2018).

[15] M. D. Bartlett, N. Kazem, M. J. Powell-Palm, X. Huang, W. Sun, J. A. Malen, and C. Majidi, High thermal conductivity in soft elastomers with elongated liquid metal inclusions, Proc. Natl. Acad. Sci. USA **114**, 2143 (2017).

[16] N. Kazem, T. Hellebrekers, and C. Majidi, Soft multifunctional composites and emulsions with liquid metals, Adv. Mater. **29**, 1605985 (2017).

[17] C. Majidi, Soft-matter engineering for soft robotics, Adv. Mater. Technol. **4**, 1800477 (2019).

[18] Y. Zhao, P. Khandagale, and C. Majidi, Modeling electromechanical coupling of liquid metal embedded elastomers while accounting stochasticity in 3D percolation, Extreme Mech. Lett. **48**, 101443 (2021).

[19] M. D. Bartlett, M. D. Dickey, and C. Majidi, Self-healing materials for soft-matter machines and electronics, NPG Asia Mater. **11**, 1 (2019).

[20] M. J. Ford, C. P. Ambulo, T. A. Kent, E. J. Markvicka, C. Pan, J. Malen, T. H. Ware, and C. Majidi, A multifunctional shape-morphing elastomer with liquid metal inclusions, Proc. Natl. Acad. Sci. USA **116**, 21438 (2019).

[21] N. Zolfaghari, P. Khandagale, M. J. Ford, K. Dayal, and C. Majidi, Network topologies dictate electromechanical coupling in liquid metal–elastomer composites, Soft Matter **16**, 8818 (2020).

[22] Y. Ohm, C. Pan, M. J. Ford, X. Huang, J. Liao, and C. Majidi, An electrically conductive silver–polyacrylamide–alginate hydrogel composite for soft electronics, Nat. Electron. **4**, 185 (2021).

[23] M. H. Malakooti, M. R. Bockstaller, K. Matyjaszewski, and C. Majidi, Liquid metal nanocomposites, Nanoscale Adv. **2**, 2668 (2020).

[24] T. H. Ware, J. S. Biggins, A. F. Shick, M. Warner, and T. J. White, Localized soft elasticity in liquid crystal elastomers, Nat. Commun. **7**, 10781 (2016).

[25] T. J. White and D. J. Broer, Programmable and adaptive mechanics with liquid crystal polymer networks and elastomers, Nat. Mater. **14**, 1087 (2015).

[26] T. H. Ware, M. E. McConney, J. J. Wie, V. P. Tondiglia, and T. J. White, Voxelated liquid crystal elastomers, Science **347**, 982 (2015).

[27] C. P. Ambulo, J. J. Burroughs, J. M. Boothby, H. Kim, M. R. Shankar, and T. H. Ware, Four-dimensional printing of liquid crystal elastomers, ACS Appl. Mater. Interfaces **9**, 37332 (2017).

[28] J. Mu, M. J. De Andrade, S. Fang, X. Wang, E. Gao, N. Li, S. H. Kim, H. Wang, C. Hou, Q. Zhang *et al.*, Sheath-run artificial muscles, Science **365**, 150 (2019).

[29] M. O. Saed, C. P. Ambulo, H. Kim, R. De, V. Raval, K. Searles, D. A. Siddiqui, J. M. O. Cue, M. C. Stefan, M. R. Shankar *et al.*, Molecularly-engineered, 4D-printed liquid crystal elastomer actuators, Adv. Funct. Mater. **29**, 1806412 (2019).

[30] J. J. Wie, M. R. Shankar, and T. J. White, Photomotility of polymers, Nat. Commun. **7**, 13260 (2016).

[31] M. Babaei, J. A. Clement, K. Dayal, and M. R. Shankar, Steering with light: indexable photomotility in liquid crystalline polymers, RSC Adv. **7**, 52510 (2017).

[32] M. Babaei, J. Gao, A. Clement, K. Dayal, and M. R. Shankar, Torque-dense photomechanical actuation, Soft Matter **17**, 1258 (2021).

[33] M. Mooney, A theory of large elastic deformation, J. Appl. Phys. **11**, 582 (1940).

[34] R. W. Ogden, *Non-Linear Elastic Deformations* (Courier Corporation, Chelmsford, 1997).

[35] A. N. Gent, A new constitutive relation for rubber, Rubber Chem. Tech. **69**, 59 (1996).

[36] H. M. James and E. Guth, Theory of the elastic properties of rubber, J. Chem. Phys. **11**, 455 (1943).

[37] P. J. Flory and J. Rehner Jr, Statistical mechanics of cross-linked polymer networks I. rubberlike elasticity, J. Chem. Phys. **11**, 512 (1943).

[38] L. R. G. Treloar, The elasticity of a network of long-chain molecules.—III, Trans. Faraday Soc. **42**, 83 (1946).

[39] L. R. G. Treloar, The photoelastic properties of short-chain molecular networks, Trans. Faraday Soc. **50**, 881 (1954).

[40] E. M. Arruda and M. C. Boyce, A three-dimensional constitutive model for the large stretch behavior of rubber elastic materials, J. Mech. Phys. Solids **41**, 389 (1993).

[41] P. D. Wu and E. V. Der Giessen, On improved network models for rubber elasticity and their applications to orientation hardening in glassy polymers, J. Mech. Phys. Solids **41**, 427 (1993).

[42] C. Miehe, S. Göktepe, and F. Lulei, A micro-macro approach to rubber-like materials—part I: The non-affine micro-sphere model of rubber elasticity, J. Mech. Phys. Solids **52**, 2617 (2004).

[43] M. Grasinger, Polymer networks which locally rotate to accommodate stresses, torques, and deformation, J. Mech. Phys. Solids **175**, 105289 (2023).

[44] G. Ronca and G. Allegra, An approach to rubber elasticity with internal constraints, J. Chem. Phys. **63**, 4990 (1975).

[45] P. J. Flory, Statistical thermodynamics of random networks, Proc. R. Soc. London A **351**, 351 (1976).

[46] P. J. Flory, Theory of elasticity of polymer networks. the effect of local constraints on junctions, J. Chem. Phys. **66**, 5720 (1977).
[47] B. Erman and P. J. Flory, Theory of elasticity of polymer networks. ii. the effect of geometric constraints on junctions, J. Chem. Phys. **68**, 5363 (1978).
[48] P. J. Flory and B. Erman, Theory of elasticity of polymer networks. 3, Macromolecules **15**, 800 (1982).
[49] R. T. Deam and S. F. Edwards, The theory of rubber elasticity, Philos. Trans. R. Soc. London A **280**, 317 (1976).
[50] S. F. Edwards and T. A. Vilgis, The tube model theory of rubber elasticity, Rep. Prog. Phys. **51**, 243 (1988).
[51] G. Heinrich and E. Straube, On the strength and deformation dependence of the tube-like topological constraints of polymer networks, melts and concentrated solutions. I. the polymer network case, Acta Polymerica **34**, 589 (1983).
[52] G. Heinrich and E. Straube, On the strength and deformation dependence of the tube-like topological constraints of polymer networks, melts and concentrated solutions. II. polymer melts and concentrated solutions, Acta Polymerica **35**, 115 (1984).
[53] G. Heinrich, E. Straube, and G. Helmis, Rubber elasticity of polymer networks: Theories, in *Polymer Physics*, Advances in Polymer Science Vol. 85 (Springer, Berlin, Heidelberg, 1988), pp. 33–87.
[54] P.-G. De Gennes, Some conformation problems for long macromolecules, Rep. Prog. Phys. **32**, 187 (1969).
[55] P.-G. De Gennes, *Scaling Concepts in Polymer Physics* (Cornell University Press, Ithaca, 1979).
[56] M. W. Matsen, Self-consistent field theory and its applications, in *Soft Matter*, edited by G. Gompper and M. Schick (Wiley-VCH, Weinheim, 2005).
[57] M. Doi and S. F. Edwards, *The Theory of Polymer Dynamics* (Oxford University Press, Oxford, 1986).
[58] G. Fredrickson, *The Equilibrium Theory of Inhomogeneous Polymers* (Oxford University Press, Oxford, 2006).
[59] G. H. Fredrickson, V. Ganesan, and F. Drolet, Field-theoretic computer simulation methods for polymers and complex fluids, Macromolecules **35**, 16 (2002).
[60] T. L. Chantawansri, A. W. Bosse, A. Hexemer, H. D. Ceniceros, C. J. Garcia-Cervera, E. J. Kramer, and G. H. Fredrickson, Self-consistent field theory simulations of block copolymer assembly on a sphere, Phys. Rev. E **75**, 031802 (2007).
[61] E. M. Lennon, K. Katsov, and G. H. Fredrickson, Free Energy Evaluation in Field-Theoretic Polymer Simulations, Phys. Rev. Lett. **101**, 138302 (2008).
[62] F. Drolet and G. H. Fredrickson, Combinatorial Screening of Complex Block Copolymer Assembly with Self-Consistent Field Theory, Phys. Rev. Lett. **83**, 4317 (1999).
[63] S. W. Sides, B. J. Kim, E. J. Kramer, and G. H. Fredrickson, Hybrid Particle-Field Simulations of Polymer Nanocomposites, Phys. Rev. Lett. **96**, 250601 (2006).
[64] D. M. Ackerman, K. Delaney, G. H. Fredrickson, and B. Ganapathysubramanian, A finite element approach to self-consistent field theory calculations of multiblock polymers, J. Comput. Phys. **331**, 280 (2017).
[65] G. H. Fredrickson, Computational field theory of polymers: Opportunities and challenges, Soft Matter **3**, 1329 (2007).
[66] K. T. Delaney and G. H. Fredrickson, Recent developments in fully fluctuating field-theoretic simulations of polymer melts and solutions, J. Phys. Chem. B **120**, 7615 (2016).
[67] E. W. Cochran, C. J. Garcia-Cervera, and G. H. Fredrickson, Stability of the gyroid phase in diblock copolymers at strong segregation, Macromolecules **39**, 2449 (2006).
[68] E. M. Lennon, G. O. Mohler, H. D. Ceniceros, C. J. García-Cervera, and G. H. Fredrickson, Numerical solutions of the complex langevin equations in polymer field theory, Multiscale Model. Simul. **6**, 1347 (2008).
[69] M. W. Matsen and M. Schick, Stable and Unstable Phases of a Diblock Copolymer Melt, Phys. Rev. Lett. **72**, 2660 (1994).
[70] M. W. Matsen, The standard Gaussian model for block copolymer melts, J. Phys.: Condens. Matter **14**, R21 (2002).
[71] F. Schmid, Self-Consistent Field Approach for Cross-Linked Copolymer Materials, Phys. Rev. Lett. **111**, 028303 (2013).
[72] L. R. G. Treloar, *The Physics of Rubber Elasticity* (Oxford University Press, New York, 1975).
[73] J. D. Davidson and N. C. Goulbourne, A nonaffine network model for elastomers undergoing finite deformations, J. Mech. Phys. Solids **61**, 1784 (2013).
[74] J. D. Davidson and N. C. Goulbourne, Nonaffine chain and primitive path deformation in crosslinked polymers, Modell. Simul. Mater. Sci. Eng. **24**, 065002 (2016).
[75] M. Rubinstein and S. Panyukov, Nonaffine deformation and elasticity of polymer networks, Macromolecules **30**, 8036 (1997).
[76] M. Rubinstein and S. Panyukov, Elasticity of polymer networks, Macromolecules **35**, 6670 (2002).
[77] B. Zimm, W. H. Stockmayer, and M. Fixman, Excluded volume in polymer chains, J. Chem. Phys. **21**, 1716 (1953).
[78] H. P. Langtangen and A. Logg, *Solving PDEs in Python: The FEniCS Tutorial I* (Springer Nature, Berlin, 2017).
[79] S. T. Milner, M.-D. Lacasse, and W. W. Graessley, Why χ is seldom zero for polymer-solvent mixtures, Macromolecules **42**, 876 (2009).
[80] J. Nistane, L. Chen, Y. Lee, R. Lively, and R. Ramprasad, Estimation of the flory-huggins interaction parameter of polymer-solvent mixtures using machine learning, MRS Commun. **12**, 1096 (2022).
[81] J. P. Wittmer, P. Beckrich, H. Meyer, A. Cavallo, A. Johner, and J. Baschnagel, Intramolecular long-range correlations in polymer melts: The segmental size distribution and its moments, Phys. Rev. E **76**, 011803 (2007).
[82] M. Lang, M. Rubinstein, and J.-U. Sommer, Conformations of a long polymer in a melt of shorter chains: Generalizations of the flory theorem, ACS Macro Lett. **4**, 177 (2015).
[83] W. Hong, X. Zhao, J. Zhou, and Z. Suo, A theory of coupled diffusion and large deformation in polymeric gels, J. Mech. Phys. Solids **56**, 1779 (2008).
[84] H. Kamata, X. Li, Ung-il Chung, and T. Sakai, Design of hydrogels for biomedical applications, Adv. Healthcare Mater. **4**, 2360 (2015).
[85] T. Tanaka and D. J. Fillmore, Kinetics of swelling of gels, J. Chem. Phys. **70**, 1214 (1979).
[86] J. Jagur-Grodzinski, Polymeric gels and hydrogels for biomedical and pharmaceutical applications, Polym. Adv. Technol. **21**, 27 (2010).
[87] M. D. A. Norman, S. A. Ferreira, G. M. Jowett, L. Bozec, and E. Gentleman, Measuring the elastic modulus of soft culture

surfaces and three-dimensional hydrogels using atomic force microscopy, Nat. Protocols **16**, 2418 (2021).

[88] V. R. Feig, H. Tran, M. Lee, and Z. Bao, Mechanically tunable conductive interpenetrating network hydrogels that mimic the elastic moduli of biological tissue, Nat. Commun. **9**, 2740 (2018).

[89] S. Xu, Z. Zhou, Z. Liu, and P. Sharma, Concurrent stiffening and softening in hydrogels under dehydration, Sci. Adv. **9**, eade3240 (2023).

[90] S. Coyle, C. Majidi, P. LeDuc, and K. J. Hsia, Bio-inspired soft robotics: Material selection, actuation, and design, Extreme Mech. Lett. **22**, 51 (2018).

[91] J. Li, Z. Suo, and J. J. Vlassak, Stiff, strong, and tough hydrogels with good chemical stability, J. Mater. Chem. B **2**, 6708 (2014).

[92] C. Sun and P. K. Purohit, Rheology of fibrous gels under compression, Extreme Mech. Lett. **54**, 101757 (2022).

[93] S. Cai, D. Breid, A. J. Crosby, Z. Suo, and J. W. Hutchinson, Periodic patterns and energy states of buckled films on compliant substrates, J. Mech. Phys. Solids **59**, 1094 (2011).

[94] W. Shan, S. Diller, A. Tutcuoglu, and C. Majidi, Rigidity-tuning conductive elastomer, Smart Mater. Struct. **24**, 065001 (2015).

[95] L. G. Lovell and C. N. Bowman, The effect of kinetic chain length on the mechanical relaxation of crosslinked photopolymers, Polymer **44**, 39 (2003).

[96] E. I. Wisotzki, M. Hennes, C. Schuldt, F. Engert, W. Knolle, U. Decker, J. A. Käs, M. Zink, and S. G. Mayr, Tailoring the material properties of gelatin hydrogels by high energy electron irradiation, J. Mater. Chem. B **2**, 4297 (2014).

[97] Y. Zhao, Y. Ohm, J. Liao, Y. Luo, H.-Y. Cheng, P. Won, P. Roberts, M. R. Carneiro, M. F. Islam, J. H. Ahn *et al.*, A self-healing electrically conductive organogel composite, Nat. Electron. **6**, 206 (2023).

[98] B. A. Krajina, A. Zhu, S. C. Heilshorn, and A. J. Spakowitz, Active DNA Olympic Hydrogels Driven by Topoisomerase Activity, Phys. Rev. Lett. **121**, 148001 (2018).

[99] J. Li, W. R. K. Illeperuma, Z. Suo, and J. J. Vlassak, Hybrid hydrogels with extremely high stiffness and toughness, ACS Macro Lett. **3**, 520 (2014).

[100] Z. Li, Z. Liu, T. Y. Ng, and P. Sharma, The effect of water content on the elastic modulus and fracture energy of hydrogel, Extreme Mech. Lett. **35**, 100617 (2020).

[101] M. C. Darnell, J.-Y. Sun, M. Mehta, C. Johnson, P. R. Arany, Z. Suo, and D. J. Mooney, Performance and biocompatibility of extremely tough alginate/polyacrylamide hydrogels, Biomaterials **34**, 8042 (2013).

[102] D. Nepal, S. Kang, K. M. Adstedt, K. Kanhaiya, M. R. Bockstaller, L. C. Brinson, M. J. Buehler, P. V. Coveney, K. Dayal, J. A. El-Awady *et al.*, Hierarchically structured bioinspired nanocomposites, Nat. Mater. **22**, 18 (2023).

[103] M. Rubinstein and R. H. Colby, *Polymer Physics*, Vol. 23 (Oxford University Press, Oxford, 2003).

[104] R. H. Pritchard and E. M. Terentjev, Swelling and de-swelling of gels under external elastic deformation, Polymer **54**, 6954 (2013).

[105] M. A. Biot, Nonlinear and semilinear rheology of porous solids, J. Geophys. Res. **78**, 4924 (1973).

[106] O. Coussy, *Poromechanics* (John Wiley & Sons, New York, 2004).

[107] J. W. Rudnicki, Coupled deformation-diffusion effects in the mechanics of faulting and failure of geomaterials, Appl. Mech. Rev. **54**, 483 (2001).

[108] M. Karimi, M. Massoudi, N. Walkington, M. Pozzi, and K. Dayal, Energetic formulation of large-deformation poroelasticity, Int. J. Numer. Anal. Methods Geomech. **46**, 910 (2022).

[109] H. Wang, *Theory of Linear Poroelasticity with Applications to Geomechanics and Hydrogeology*, Vol. 2 (Princeton University Press, Princeton, 2000).

[110] G. Grekas, M. Proestaki, P. Rosakis, J. Notbohm, C. Makridakis, and G. Ravichandran, Cells exploit a phase transition to mechanically remodel the fibrous extracellular matrix, J. R. Soc. Interface **18**, rsif.2020.0823 (2021).

[111] R. Lakes, P. Rosakis, and A. Ruina, Microbuckling instability in elastomeric cellular solids, J. Mater. Sci. **28**, 4667 (1993).

[112] C. Sun, I. N. Chernysh, J. W. Weisel, and P. K. Purohit, Fibrous gels modelled as fluid-filled continua with double-well energy landscape, Proc. R. Soc. A **476**, 20200643 (2020).

[113] https://github.com/pkhandag/polymer-network.git